Theoretical analysis on lower band cascade as a mechanism for multiband chorus in the Earth's magnetosphere

Xinliang Gao, Quanming Lu, Shaojie Wang, and Shui Wang

Citation: AIP Advances **8**, 055003 (2018); doi: 10.1063/1.5025507
View online: https://doi.org/10.1063/1.5025507
View Table of Contents: http://aip.scitation.org/toc/adv/8/5
Published by the American Institute of Physics

Theoretical analysis on lower band cascade as a mechanism for multiband chorus in the Earth's magnetosphere

Xinliang Gao,[1,2] Quanming Lu,[1,2,a] Shaojie Wang,[1,3] and Shui Wang[1,2]
[1]*CAS Key Laboratory of Geospace Environment, Department of Geophysics and Planetary Science, University of Science and Technology of China, Hefei 230026, China*
[2]*Collaborative Innovation Center of Astronautical Science and Technology, Harbin 150001, China*
[3]*Department of Modern Physics, University of Science and Technology of China, Hefei 230026, China*

(Received 9 February 2018; accepted 23 April 2018; published online 2 May 2018)

Whistler-mode waves play a crucial role in controlling electron dynamics in the Earth's Van Allen radiation belt, which is increasingly important for spacecraft safety. Using THEMIS waveform data, Gao et al. [X. L. Gao, Q. Lu, J. Bortnik, W. Li, L. Chen, and S. Wang, Geophys. Res. Lett., 43, 2343-2350, 2016] have reported two multiband chorus events, wherein upper-band chorus appears at harmonics of lower-band chorus. They proposed that upper-band harmonic waves are excited through the nonlinear coupling between the electromagnetic and electrostatic components of lower-band chorus, a second-order effect called "lower band cascade". However, the theoretical explanation of lower band cascade was not thoroughly explained in the earlier work. In this paper, based on a cold plasma assumption, we have obtained the explicit nonlinear driven force of lower band cascade through a full nonlinear theoretical analysis, which includes both the ponderomotive force and coupling between electrostatic and electromagnetic components of the pump whistler wave. Moreover, we discover the existence of an efficient energy-transfer (E-t) channel from lower-band to upper-band whistler-mode waves during lower band cascade for the first time, which is also confirmed by PIC simulations. For lower-band whistler-mode waves with a small wave normal angle (WNA), the E-t channel is detected when the driven upper-band wave nearly satisfies the linear dispersion relation of whistler mode. While, for lower-band waves with a large WNA, the E-t channel is found when the lower-band wave is close to its resonant frequency, and the driven upper-band wave becomes quasi-electrostatic. Through this efficient channel, the harmonic upper band of whistler waves is generated through energy cascade from the lower band, and the two-band spectral structure of whistler waves is then formed. Both two types of banded whistler-mode spectrum have also been successfully reproduced by PIC simulations.
https://doi.org/10.1063/1.5025507

I. INTRODUCTION

Whistler-mode waves are one of the most significant natural emissions in the Earth's magnetosphere, as they are believed to play a key role in regulating electron dynamics in the Van Allen radiation belt.[1–5] These waves are believed to be a dominant source of "killer electrons" (~MeV) in Earth's magnetosphere,[3,5,6] which is a major threat to astronauts and operating satellites. Furthermore, they are also the primary contributor of strong diffuse auroral precipitation into the Earth's atmosphere,[2,7] resulting in enhanced chemical changes of the atmosphere.[2] One of the most salient characteristics

[a]email: qmlu@ustc.edu.cn

of whistler-mode waves in the magnetosphere is that they often exhibit a two-band spectral structure,[8] separated by a power gap around $0.5f_{ce}$ (where f_{ce} is the equatorial electron gyrofrequency): lower band (0.1-0.5 f_{ce}) and upper band (0.5-0.8 f_{ce}).

The two-band spectral structure of whistler-mode waves in the magnetosphere was identified almost 40 years ago.[8] The lower band of whistler-mode waves has been commonly believed to be excited by hot (~keV) anisotropic electrons injected from the plasmas sheet.[9–11] Moreover, whistler-mode waves with the frequency chirping, also named as chorus, are considered to be excited in a nonlinear way, which is closely correlated with the nonlinear trapping of resonant electrons.[12,13] However, the generation mechanism of upper-band whistler-mode waves is still in debate.[13–15] The more direct and traditional idea is that upper-band whistler-mode waves can be either linearly or nonlinearly generated by anisotropic warm (~100s eV) electrons just like lower-band waves,[13,14] but this requires an unrealistic temperature anisotropy in the magnetosphere.[15] Based on THEMIS waveform data, Gao et al.[15] have reported two multiband whistler-mode events, where upper-band waves are found to be the second harmonic of lower-band waves, i.e., at twice the frequency of the lower-band wave. Lower-band and upper-band harmonic waves are observed to have the same wave normal angle and the same propagating direction, while, the magnetic amplitude of upper-band harmonic waves is 1-2 orders of magnitude smaller than that of lower-band chorus. They proposed that upper-band waves are excited through the coupling between the electromagnetic and electrostatic components of lower-band whistler waves (i.e., lower band cascade), which could be a potential generation mechanism of upper-band whistler-mode waves in the Earth's magnetosphere.

However, a full nonlinear theoretical explanation of lower band cascade was not provided in the earlier work, and the question whether sufficient energy can be transferred to the upper band was not addressed. In this paper, based on theoretical analysis, we derive the explicit nonlinear driven force of lower band cascade, and predict the existence of an efficient channel for energy transfer during the cascade from lower-band to upper-band whistler-mode waves. The existence of an efficient channel is also verified by particle-in-cell simulations. We conclude that lower band cascade explains the generation of upper-band waves when the upper-band frequencies are integer multiples of the lower-band frequency in the magnetosphere.

II. THEORETICAL ANALYSIS ON LOWER BAND CASCADE

To simplify the underlying physics, we assume a uniform cold proton-electron plasma. Since the frequency of the whistler mode is much larger than the proton gyrofrequency, protons are assumed to be a motionless. Electrons are treated as a fluid since kinetic effects are not important here. So, our basic equations conserve mass and momentum for electrons,

$$\partial_t n_e + \nabla \cdot (n_e \mathbf{v_e}) = 0 \tag{1}$$

$$m_e(\partial_t \mathbf{v_e} + \mathbf{v_e} \cdot \nabla \mathbf{v_e}) = -e(\mathbf{E} + \mathbf{v_e} \times \mathbf{B}) \tag{2}$$

and Maxwell's equations,

$$\nabla \cdot \mathbf{E} = -\frac{1}{\varepsilon_0}(n_e - n_0)e \tag{3}$$

$$\nabla \times \mathbf{B} = -\mu_0 n_e e \mathbf{v_e} + \frac{1}{c^2}\partial_t \mathbf{E} \tag{4}$$

$$\nabla \times \mathbf{E} = -\partial_t \mathbf{B} \tag{5}$$

where n_e, $\mathbf{v_e}$, e and n_0 are electron density, electron velocity, proton charge and proton density, respectively. For convenience, we establish a new Cartesian coordinate, where the x axis is along the wave vector, the y axis is lying in the plane defined by the wave vector and background magnetic field, and z axis completes the right-hand coordinate system.

To linearize equations (1)–(5), all physical quantities are assumed to be the superposition of equilibrium and perturbed terms:

$$\begin{cases} n_e = n_0 + (\delta n' + \delta n'') \\ \mathbf{v_e} = (\delta v'_{\parallel} + \delta v''_{\parallel})\hat{\mathbf{x}} + (\delta v'_{\perp y} + \delta v''_{\perp y})\hat{\mathbf{y}} + (\delta v'_{\perp z} + \delta v''_{\perp z})\hat{\mathbf{z}} \\ \mathbf{E} = (\delta E'_{\parallel} + \delta E''_{\parallel})\hat{\mathbf{x}} + (\delta E'_{\perp y} + \delta E''_{\perp y})\hat{\mathbf{y}} + (\delta E'_{\perp z} + \delta E''_{\perp z})\hat{\mathbf{z}} \\ \mathbf{B} = B_0(\cos\theta\hat{\mathbf{x}} + \sin\theta\hat{\mathbf{y}}) + (\delta b'_{\perp y} + \delta b''_{\perp y})\hat{\mathbf{y}} + (\delta b'_{\perp z} + \delta b''_{\perp z})\hat{\mathbf{z}} \end{cases} \tag{6}$$

where θ is the wave normal angle. First-order perturbations with a prime represent the lower-band whistler-mode wave, while second-order perturbations with a double prime represent the upper-band harmonic wave. This method is similar to that described by Tsytovich.[16] The field perturbation $\delta E'_{\parallel}$ and velocity perturbation $\delta v'_{\parallel}$ along with the density perturbation $\delta n'$ represent the electrostatic component of the lower-band whistler mode, while the perpendicular components of the primed perturbations represent its electromagnetic component.

Since lower band cascade is a nonlinear physical process, we will keep terms up to the second order when equation (6) is inserted into equations (1)–(5). This means that we retain products of the first-order perturbations (primed variables) with each other and products of the second-order perturbations (double-primed variables) only with the equilibrium terms. All first-order perturbations are assumed to have the form $\sim e^{-i(\omega t - \mathbf{k}\cdot\mathbf{x})}$, while second-order terms necessarily have the form $\sim e^{-i(2\omega t - 2\mathbf{k}\cdot\mathbf{x})}$ since they must be equated with products of the first-order terms. Inserting equation (6) into equations (1)–(5) and solving for the terms involving $\sim e^{-i(\omega t - \mathbf{k}\cdot\mathbf{x})}$ yields the linear dispersion relation of whistler-mode waves,

$$\left(\frac{1}{c^2\Omega_e}\omega^2 k - \frac{\Omega_e}{V_{Ae}^2}k\right)\left[\left(\cos\theta k^2 - \frac{\cos\theta}{c^2}\omega^2\right)^2 - \left(\frac{1}{c^2\Omega_e}\omega^3 - \frac{1}{\Omega_e}\omega k^2 - \frac{\Omega_e}{V_{Ae}^2}\omega\right)^2\right]$$
$$-\left(\sin\theta k^2 - \frac{1}{c^2}\sin\theta\omega^2\right)\frac{1}{c^2}\sin\theta\omega k\left(\frac{1}{c^2\Omega_e}\omega^3 - \frac{1}{\Omega_e}\omega k^2 - \frac{\Omega_e}{V_{Ae}^2}\omega\right) = 0 \tag{7}$$

and solving the terms involving $\sim e^{-i(2\omega t - 2\mathbf{k}\cdot\mathbf{x})}$ yields the governing equation of lower band cascade,

$$\begin{bmatrix} i\frac{8}{c^2\Omega_e}\omega^2 k - i\frac{2\Omega_e}{V_{Ae}^2}k & 4\sin\theta k^2 - \frac{4}{c^2}\sin\theta\omega^2 & 0 \\ 0 & 4\cos\theta k^2 - \frac{4\cos\theta}{c^2}\omega^2 & \begin{bmatrix} -i\frac{8}{c^2\Omega_e}\omega^3 + i\frac{8}{\Omega_e}\omega k^2 \\ +i\frac{2\Omega_e}{V_{Ae}^2}\omega \end{bmatrix} \\ \frac{4}{c^2}\sin\theta\omega k & \begin{bmatrix} i\frac{8}{c^2\Omega_e}\omega^3 - i\frac{8}{\Omega_e}\omega k^2 \\ -i\frac{2\Omega_e}{V_{Ae}^2}\omega \end{bmatrix} & 4\cos\theta k^2 - \frac{4\cos\theta}{c^2}\omega^2 \end{bmatrix} \begin{bmatrix} \delta E''_{\parallel} \\ \delta b''_{\perp y} \\ \delta b''_{\perp z} \end{bmatrix} = NL$$

$$NL = \begin{bmatrix} \begin{bmatrix} -2\frac{B_0}{V_{Ae}^2}k^2\left(\delta v'_{\parallel}\delta v'_{\parallel}\right) + i2\frac{\Omega_e}{V_{Ae}^2}k\left(\delta v'_{\perp y}\delta b'_{\perp z} - \delta v'_{\perp z}\delta b'_{\perp y}\right) \\ +i2\frac{B_0}{n_0}\frac{\Omega_e}{V_{Ae}^2}\sin\theta k\left(\delta n'\delta v'_{\perp z}\right) - 4\frac{B_0}{n_0}\frac{1}{V_{Ae}^2}\omega k\left(\delta n'\delta v'_{\parallel}\right) \end{bmatrix} \\ \begin{bmatrix} 2\frac{B_0}{V_{Ae}^2}k^2\left(\delta v'_{\parallel}\delta v'_{\perp y}\right) + i2\frac{\Omega_e}{V_{Ae}^2}k\left(\delta b'_{\perp z}\delta v'_{\parallel}\right) \\ +i2\frac{B_0}{n_0}\frac{\Omega_e}{V_{Ae}^2}\cos\theta k\left(\delta n'\delta v'_{\perp z}\right) + 4\frac{B_0}{n_0}\frac{1}{V_{Ae}^2}\omega k\left(\delta n'\delta v'_{\perp y}\right) \end{bmatrix} \\ \begin{bmatrix} 2\frac{B_0}{V_{Ae}^2}k^2\left(\delta v'_{\parallel}\delta v'_{\perp z}\right) - i2\frac{\Omega_e}{V_{Ae}^2}k\left(\delta b'_{\perp y}\delta v'_{\parallel}\right) + 4\frac{B_0}{n_0}\frac{1}{V_{Ae}^2}\omega k\left(\delta n'\delta v'_{\perp z}\right) \\ +2i\frac{B_0}{n_0}\frac{\Omega_e}{V_{Ae}^2}k\left(\delta n'\delta v'_{\parallel}\sin\theta - \delta n'\delta v'_{\perp y}\cos\theta\right) \end{bmatrix} \end{bmatrix} \tag{8}$$

where ω and k are the frequency and wave number of the lower-band whistler-mode wave, c is the light speed, Ω_e is the electron gyrofrequency, and V_{Ae} is defined as $\sqrt{\frac{B_0^2}{\mu_0 n_0 m_e}}$.

Based on a cold plasma model, we have derived the governing equation (Eq. (8)) of lower band cascade, where the pump wave satisfying equation (7) is assumed as a monochromatic whistler mode. The right side of the governing equation gives the nonlinear driven force, which indicates the electrostatic component of the lower-band whistler-mode wave is important and necessary for exciting upper-band harmonic waves. This means upper-band waves will not be excited if the lower-band whistler-mode wave is strictly parallel to the background magnetic field. For the parallel electric field of the upper-band wave, the nonlinear driven force is equivalent to the ponderomotive force. While, for its perpendicular magnetic fields, the nonlinear driven force results from the coupling between the electrostatic and electromagnetic components of the lower-band whistler-mode wave.

Here, we assume the ratio of plasma frequency to electron gyrofrequency is 4, which are typical values in the magnetosphere.[17] Based on Eqs. (1)–(8), with a given magnetic amplitude of the lower-band whistler-mode wave, we can obtain their amplitude ratios ($\delta E_{\|H}/\delta E_{\|L}$ and $\delta B_H/\delta B_L$), which can quantify the energy-transfer efficiency from lower-band to upper-band harmonic waves. For lower-band whistler waves, they usually have small wave normal angles ($\leq 30^o$), but there is also a significant population with large wave normal angles ($\geq 60^o$).[18] Therefore, two types of typical lower-band whistler wave are chosen: type I with a small WNA (30^o) and a larger magnetic amplitude ($0.01B_0$); type II with a large WNA (70^o) and a smaller magnetic amplitude ($0.001B_0$). For type I lower-band wave, there is a very clear but narrow frequency region (shaded in green) with extremely large amplitude ratios ($>10^{-2}$) in Fig. 1(a), which is called as the energy-transfer (E-t) channel here. More interestingly, within this E-t channel, the excited upper-band waves are found to nearly satisfy the linear dispersion relation of whistler-mode waves (Fig. 1(b)). Therefore, this will result in an extremely small determinant of the coefficient matrix on the left hand of Eq. (8), and the amplitude of the upper-band wave can become very large even if the nonlinear driven force is only moderate. In short, if the excited upper-band harmonic wave is also a normal mode in this system, the energy transfer from lower-band to upper-band waves will become very efficient. However, for type II lower-band whistler-mode wave, it is a very different case. Now the efficient E-t channel is found when the lower-band wave is close to its resonant frequency ($\sim\cos 70^o\Omega_{ce}$) in Fig. 2(a), and the excited upper-band harmonic waves within the E-t channel are just driven modes rather than normal modes in this plasma (Fig. 2(b)). The very oblique lower-band whistler mode typically has a small magnetic amplitude, but its electrostatic component and wave number can be quite large if its frequency is close to the resonant frequency. As a result, the nonlinear driven force on the right side of Eq. (8) will become very strong, and the excited upper-band harmonic wave can gain much energy.

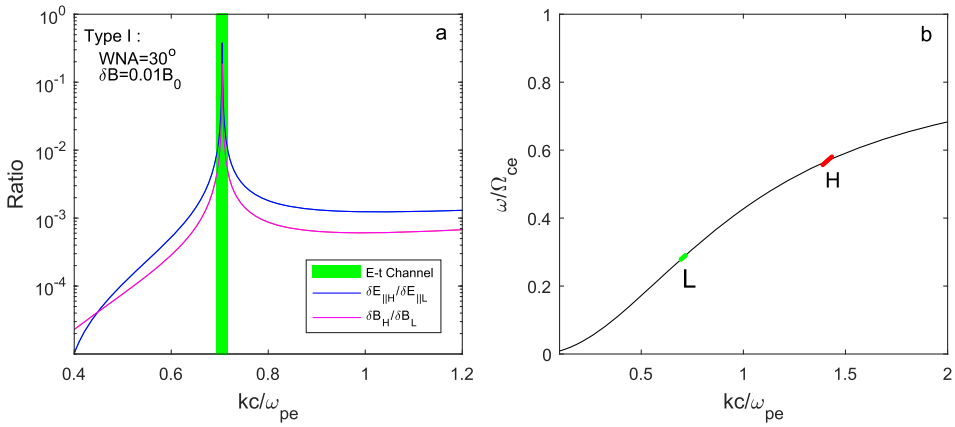

FIG. 1. In panel a, the E-t channel is shaded in green, where $\delta E_{\|H}/\delta E_{\|L}$ is larger than 10^{-2}. Subscripts "L" and "H" represent the lower-band and upper-band harmonic waves, respectively. In panel b, the lower-band waves and the driven upper-band waves within the E-t channel are denoted by green and red thick lines, respectively.

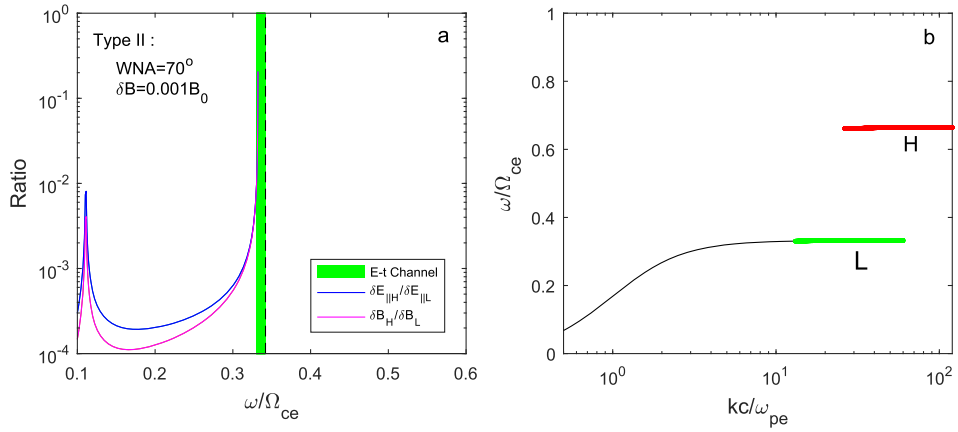

FIG. 2. (a) Electric ($\delta E_{\|H}/\delta E_{\|L}$) and magnetic ($\delta B_H/\delta B_L$) amplitude ratios as a function of wave numbers, and (b) the dispersion relation for type II whistler-mode waves with the same format as that in Figure 1.

The reported multiband chorus events in the Earth's magnetosphere[15] may belong to type I whistler waves, where the banded structure can be observed in both electric and magnetic spectrograms. While, for type II whistler waves, since their magnetic amplitude is usually very small (~10pT), so the magnetic amplitude of excited upper-band waves will be too small (~1pT) to be measured by satellites, even though the energy-transfer efficiency can be very large within the E-t channel. Therefore, for type II waves, the banded structure can only be observed in the electric spectrogram, which could be a new type of banded whistler-mode spectrum.

III. SIMULATION MODEL AND INITIAL SETUP

The particle-in-cell (PIC) simulation model is a powerful tool to study nonlinear physical processes in space plasma.[19–21] With a 1-D PIC simulation model, we have successfully reproduced two types of E-t channels. The 1-D PIC simulation model is performed in a homogeneous and collisionless electron-proton plasma, which only allows the spatial variation in the x direction. In this model, full dynamics of electrons are retained by solving the relativistic motion equation of each electron driven by the Lorentz force. While, protons are motionless by setting their mass infinite, since the proton gyrofrequency is much smaller than the frequency of whistler-mode waves. For each species, there are on average 10,000 macroparticles in every cell. The background magnetic field is lying in the x-y plane, which is given by $\mathbf{B} = B_0(\cos\theta\hat{\mathbf{x}} + \sin\theta\hat{\mathbf{y}})$ (where θ is the wave normal angle). In our simulations, the time and space have been normalized by the inverse of Ω_e and the electron inertial length $\lambda_e = c/\omega_{pe}$, where ω_{pe} is the plasma frequency. The total simulation time is $2{,}000\Omega_e^{-1}$ with a time step of $\Delta t = 0.005\Omega_e^{-1}$. There are 18 runs performed in this study, whose other useful parameters have been listed in Table I. Here, we also choose the ratio of plasma frequency to electron

TABLE I. Some useful parameters for two types of lower-band whistler-mode waves.

Type I: WNA=30°, δB=0.1B_0, Δx=0.05 λ_e				Type II: WNA=70°, δB=0.01 B_0, Δx=0.03λ_e			
R#	kc/ω_{pe}	$\delta B_H/\delta B_L$	$\delta B_H/\delta B_L{}^*$	R#	kc/ω_{pe}	$\delta E_H/\delta E_L$	$\delta E_H/\delta E_L{}^*$
1	0.60	0.0038	0.0029	1	2.12	0.0032	0.0037
2	0.65	0.0082	0.0074	2	2.58	0.0049	0.0049
3	0.69	0.0305	0.0336	3	3.00	0.0059	0.0063
4	0.7	0.0719	0.1020	4	3.67	0.0085	0.0089
5	0.704	0.2141	0.3558	5	5.01	0.0151	0.0156
6	0.709	0.1832	0.1629	6	6.54	0.0247	0.0257
7	0.72	0.0404	0.0374	7	11.60	0.0846	0.0783
8	0.75	0.0144	0.0146	8	15.00	0.1325	0.1301
9	0.80	0.0079	0.0087	9	20.00	0.2283	0.2305

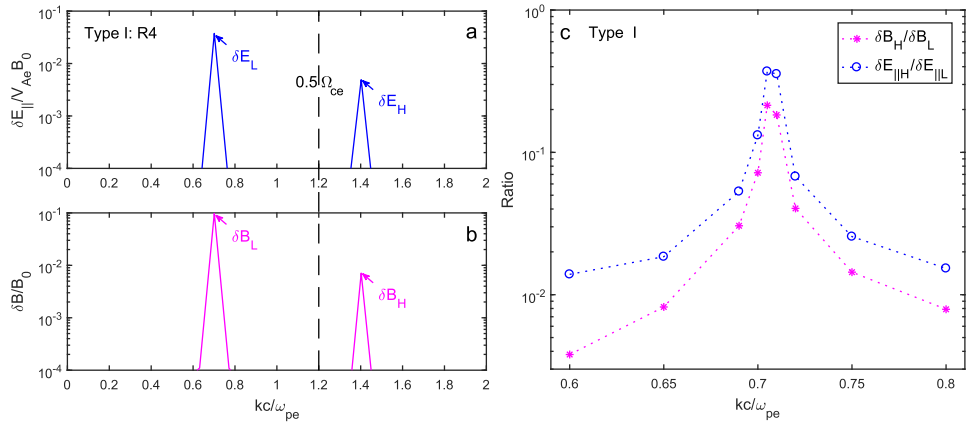

FIG. 3. (a,b) Electric and magnetic spectra as a function of wave number for R4 in type I. (c) Electric and magnetic amplitude ratios as a function of wave number for type I. The black dashed lines mark the wave number for $0.5\Omega_{ce}$, which is obtained based the linear dispersion relation. Each simulation run is denoted by "o" and "∗".

gyrofrequency to be 4. With the same method as Gao et al.,[21] a pump lower-band whistler-mode wave is initially set up by assigning fluctuating wave fields on each grid and fluctuating bulk velocity to each particle based on the linear theory. Note that, for saving computation resources, the amplitude of the pump lower-band wave has been artificially amplified in simulations.

IV. SIMULATION RESULTS

In Figs. 3(a) and 3(b), R4 of type I reproduces a typical banded whistler-mode spectrum, where two-band structure is observed in both electric and magnetic spectrograms. Most of all, the efficient E-t channel predicted above is indeed observed in Fig. 3(c), in which amplitude ratios become very large. In R7 of type II, the parallel electric field of the lower-band wave is even larger than that in R4 of type I (Fig. 4(a)), although its magnetic amplitude is one order smaller than that in R4 of type I (Figs. 3(b) and 4(b)). Therefore, this will exhibit as a new banded whistler-mode spectrum, which has already been theoretically predicted above. Moreover, there is a very clear trend that amplitude ratios increase rapidly with the frequency of the lower-band wave, especially when its frequency is approaching the resonant frequency (Fig. 4(c)). This efficient E-t channel is also consistent with that shown in Fig. 2(a). Moreover, we have listed all obtained amplitudes ratios ($\delta B_H/\delta B_L$ or $\delta E_H/\delta E_L$) in Table I, which are calculated when the amplitude of upper-band waves reaches its maximum, as well

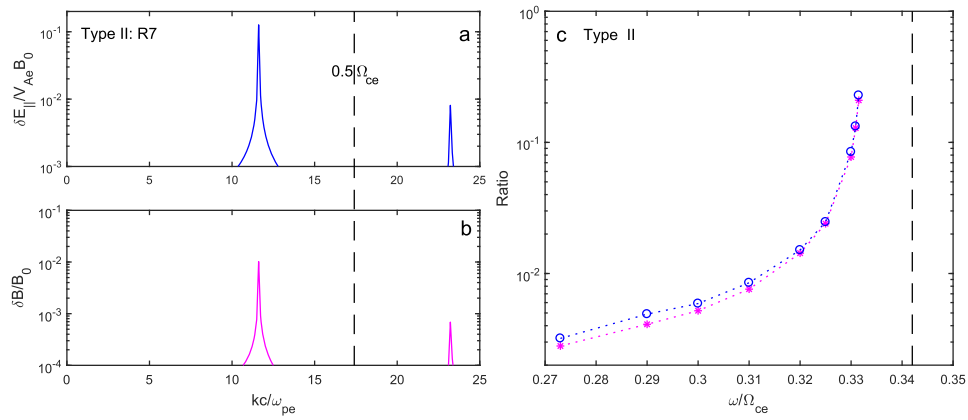

FIG. 4. (a,b) Electric and magnetic spectra as a function of wave number for R7 in type II. (c) Electric and magnetic amplitude ratios as a function of wave number for type II. The black dashed lines mark the wave number for $0.5\Omega_{ce}$, which is estimated through the linear interpolation. Each simulation run is denoted by "o" and "∗".

as theoretical values ($\delta B_H/\delta B_L{}^*$ or $\delta E_H/\delta E_L{}^*$). The amplitude ratios obtained from both simulations and theory are found to be quite consistent. Note that the obtained amplitude ratio in R5 of type I is relatively smaller than the theoretical value, which is just due to the fact that the excited upper-band harmonic wave in R5 is still growing even at the end of the simulation ($2{,}000\Omega_e^{-1}$).

V. CONCLUSIONS AND DISCUSSION

Based on theoretical analysis, we have obtained the explicit nonlinear driven force of lower band cascade in a cold plasma, which includes both the ponderomotive force and coupling between electrostatic and electromagnetic components of the pump whistler wave. Moreover, we have also predicted there exists an efficient channel for energy transfer during the cascade from lower-band to upper-band whistler-mode waves. And such kind of efficient channel is then verified by full particle simulations. For lower-band whistler-mode wave with a small wave normal angle (WNA), the E-t channel is detected when the excited harmonic upper-band wave nearly satisfies the linear dispersion relation of whistler-mode waves. While, for lower-band waves with a large WNA, the E-t channel is found when the lower-band wave is close to its resonant frequency, and the driven harmonic upper-band wave becomes quasi-electrostatic. Through the efficient E-t channel, upper-band whistler waves are able to extract sufficient energy from lower-band waves, which could be an important mechanism for generating upper-band whistler waves in Earth's magnetosphere. Both two types of banded whistler-mode spectrum have also been successfully reproduced by simulations.

Based on these results, we have further proposed a possible evolution pattern of the whistler-mode spectrum in the Earth's magnetosphere. In the equatorial plane, the parallel counter-propagating whistler waves (either discrete or hiss-like emissions) are excited by anisotropic hot electrons, then these waves propagate to relatively higher-latitude regions and their WNA can become non-zero but a small value.[22,23] Through the type I E-t channel, the whistler-mode spectrum can turn into a banded one, where lower-band and upper-band chorus waves coexist in both electric and magnetic spectrograms. At even higher-latitude regions, lower-band whistler waves can become very oblique and quasi-electrostatic,[22] which typically have a small magnetic amplitude but a large electric amplitude. In this case, the new type banded whistler-mode spectrum will be formed through the type II E-t channel. As a summary, our study not only provides a potential explanation of mysterious two-band spectra of whistler waves, but also gives a new insight into the global model of whistler-mode spectra in the Earth's magnetosphere.

ACKNOWLEDGMENTS

This work was supported by the NSFC grant 41774151, 41631071, 41604128, 41474125, Youth Innovation Promotion Association of Chinese Academy of Sciences (No. 2016395), and Key Research Program of Frontier Sciences, CAS (QYZDJ-SSW-DQC010). The simulation data will be preserved on a long-term storage system and will be made available upon request to the corresponding author.

[1] R. B. Horne and R. M. Thorne, "Relativistic electron acceleration and precipitation during resonant interactions with whistler-mode chorus," Geophys. Res. Lett. **30**(10), 1527, https://doi.org/10.1029/2003GL016973 (2003).
[2] R. M. Thorne, B. Ni, X. Tao, R. B. Horne, and N. P. Meredith, "Scattering by chorus waves as the dominant cause of diffuse auroral precipitation," Nature **467**, 943 (2010).
[3] R. M. Thorne *et al.*, "Rapid local acceleration of relativistic radiation-belt electrons by magnetospheric chorus," Nature **504**, 411 (2013).
[4] G. D. Reeves *et al.*, "Electron acceleration in the heart of the Van Allen radiation belts," Science **341**, 991–994 (2013).
[5] D. Mourenas, A. Artemyev, O. Agapitov, and V. Krasnoselskikh, "Consequences of geomagnetic activity on energization and loss of radiation belt electrons by oblique chorus waves," J. Geophys. Res. Space Physics **119**, 2775–2796, https://doi.org/10.1002/2013JA019674 (2014).
[6] F. Xiao *et al.*, "Chorus acceleration of radiation belt relativistic electrons during March 2013 geomagnetic storm," J. Geophys. Res. **119**, 3325–3332, https://doi.org/10.1002/2014ja019822 (2014).
[7] B. B. Ni, R. M. Thorne, Y. Y. Shprits, K. G. Orlova, and N. P. Meredith, "Chorus-driven resonant scattering of diffuse auroral electrons in nondipolar magnetic fields," J. Geophys. Res. **116**, A06225, https://doi.org/10.1029/2011ja016453 (2011).
[8] W. J. Burtis and R. A. Helliwell, "Banded chorus a new type of VLF radiation observed in the magnetosphere by OGO 1 and OGO 3," J. Geophys. Res. **74**(11), 3002–3010, https://doi.org/10.1029/JA074i011p03002 (1969).

[9] C. F. Kennel and H. E. Petschek, "Limit on stably trapped particle fluxes," J. Geophys. Res. **71**, 1–28, https://doi.org/10.1029/jz071i001p00001 (1966).
[10] S. P. Gary, D. Winske, and M. Hesse, "Electron temperature anisotropy instabilities: Computer simulations," J. Geophys. Res. **105**, 10751, https://doi.org/10.1029/1999ja000322 (2000).
[11] W. Li, R. M. Thorne, V. Angelopoulos, J. W. Bonnell, J. P. McFadden, C. W. Carlson, O. LeContel, A. Roux, K. H. Glassmeier, and H. U. Auster, "Evaluation of whistler-mode chorus intensification on the nightside during an injection event observed on the THEMIS spacecraft," J. Geophys. Res. **114**, A00C14, https://doi.org/10.1029/2008ja013554 (2009).
[12] Y. Omura, Y. Katoh, and D. Summers, "Theory and simulation of the generation of whistler mode chorus," J. Geophys. Res. **113**(A4), A04223, https://doi.org/10.1029/2007ja012622 (2008).
[13] Y. Omura, M. Hikishima, Y. Katoh, D. Summers, and S. Yagitani, "Nonlinear mechanisms of lower-band and upper-band VLF chorus emissions in the magnetosphere," J. Geophys. Res. **114**, A07217, https://doi.org/10.1029/2009ja014206 (2009).
[14] X. Fu *et al.*, "Whistler anisotropy instabilities as the source of banded chorus: Van Allen probes observations and particle-in-cell simulations," J. Geophys. Res. **119**, 8288, https://doi.org/10.1002/2014ja020364 (2014).
[15] X. L. Gao, Q. M. Lu, J. Bortnik, W. Li, L. J. Chen, and S. Wang, "Generation of multiband chorus by lower band cascade in the Earth's magnetosphere," Geophys. Res. Lett. **43**, 2343–2350, https://doi.org/10.1002/2016GL068313 (2016).
[16] V. N. Tsytovich, *"Nonlinear effects in plasma* (Springer, Boston, MA, 1970).
[17] X. L. Gao, W. Li, R. M. Thorne, J. Bortnik, V. Angelopoulos, Q. M. Lu, X. Tao, and S. Wang, "Statistical results describing the bandwidth and coherence coefficient of whistler mode wave suing THEMIS waveform data," J. Geophys. Res. **119**, 8992–9003, https://doi.org/10.1002/2014ja020158 (2014).
[18] W. Li, J. Bortnik, R. M. Thorne, C. M. Cully, L. Chen, V. Angelopoulos, Y. Nishimura, J. B. Tao, J. W. Bonnell, and O. Le Contel, "Characteristics of the poynting flux and wave normal vectors of whistler-mode waves observed on THEMIS," J. Geophys. Res. Space Physics **118**, 1461–1471, https://doi.org/10.1002/jgra.50176 (2013).
[19] S. Lu, V. Angelopoulos, and H. Fu, "Suprathermal particle energization in dipolarization fronts: Particle-in-cell simulations," J. Geophys. Res. Space Physics **121**, 9483–9500, https://doi.org/10.1002/2016ja022815 (2016).
[20] X. R. Fu, S. P. Gary, G. D. Reeves, D. Winske, and J. R. Woodroffe, "Generation of highly oblique lower-band chorus via nonlinear three-wave resonance," Geophys. Res. Lett. **44**, 9532–9538, https://doi.org/10.1002/2017GL074411 (2017).
[21] X. L. Gao, Y. G. Ke, Q. M. Lu, L. J. Chen, and S. Wang, "Generation of multiband chorus in the earth's Magnetosphere: 1-D PIC simulation," Geophys. Res. Lett. **44**, 618–624, https://doi.org/10.1002/2016GL072251 (2017).
[22] L. Chen, R. M. Thorne, W. Li, and J. Bortnik, "Modeling the wave normal distribution of chorus waves," J. Geophys. Res. Space Physics **118**, 1074–1088, https://doi.org/10.1029/2012JA018343 (2013).
[23] Y. G. Ke, X. Gao, Q. Lu, X. Wang, and S. Wang, "Generation of rising-tone chorus in a two-dimensional mirror field by using the general curvilinear PIC code," J. Geophys. Res. Space Physics **122**, https://doi.org/10.1002/2017JA024178 (2017).